Digital Signal Processing 62 (2017) 187–196

Contents lists available at ScienceDirect

Digital Signal Processing

www.elsevier.com/locate/dsp

DOA estimation based on multi-resolution difference co-array perspective ☆

Jianyan Liu [a,b], Yanmei Zhang [a], Yilong Lu [b], Weijiang Wang [a,*]

[a] School of Information and Electronics, Beijing Institute of Technology, Beijing 100081, PR China
[b] School of Electrical and Electronic Engineering, Nanyang Technological University, 639798, Singapore

ARTICLE INFO

Article history:
Available online 14 December 2016

Keywords:
Direction of arrival estimation
K-level co-prime array
Multi-resolution difference co-array
Spatial aliasing
Probability decision

ABSTRACT

This paper presents two kinds of K-level co-prime linear array geometries and the corresponding direction of arrival estimation algorithm based on the multi-resolution difference co-array (MRDCA) perspective. The MRDCA can simultaneously improve the degree of freedom and the angle-resolution by utilizing a class of virtual sparse uniform linear arrays generated by vectorizing the covariance matrix of the received observations of the K-level large scale sparse array. Compared to the prior two level co-prime/nested arrays, the aperture and the angle-resolution can be significantly increased with Kth power law for the K-level array, while the dimension of its scanning space is reduced to $1/K$ resulted from the spatial aliasing of the MRDCA. As a result, a low-complexity DOA estimation algorithm is proposed by combining a multi-resolution estimation at each level of sparse MRDCA and a followed probability decision strategy which aims at effectively identifying the genuine DOAs and excluding the replicas. In the end, the simulation results are provided to numerically validate the performance of the proposed array geometries.

1. Introduction

Direction of arrival (DOA) estimation is a critical problem in array signal processing. In the past few decades, many high-resolution subspace fitting approaches (e.g. MUSIC [1], ESPRIT [2] and their variants) have been proposed mainly based on overdetermined model (more sensors than sources) and uniform linear arrays (ULAs) with spacing of around half a wavelength to avoid spatial aliasing. In such a situation, to achieve very high angle-resolution and/or detect many sources with a ULA, it requires a very large aperture with massive antenna elements, which leads to formidable system complexity and costs. Therefore, some non-uniform linear arrays (NLAs) have been introduced into array signal processing field, dating back to minimum-redundancy arrays (MRAs) [3]. By directly constructing an augmented covariance matrix [4,5] or indirectly utilizing the transformation of the augmented matrix into a positive definite Toeplitz matrix [6], such MRAs allow adjacent physical element spacing to be greater than half a wavelength and also provide a solution to detect more sources than sensors. Recently, the introduction of nested array in [7] and co-prime array in [8] (their variants: super nested array [9,10], generalized co-prime array [11] and fourth-order based co-prime array [12]) has created renewed interest in NLAs. A new difference co-array (DCA) perspective for underdetermined array signal model is provided in [7] by directly vectorizing the covariance matrix of the measurements from such NLAs. This vectorized signal can be viewed as an output from a virtual array whose element positions are defined by difference positions of physical sensors. Therefore, many array signal processing algorithms, such as DOA estimation and beam-forming, can be performed based on such virtual co-arrays instead of physical arrays. As a result, the corresponding degrees of freedom (DOFs) (enhanced from $O(N)$ to $O(N^2)$) allow to find more sources than sensors [13]. Furthermore, multi-frequency techniques have been proposed in [14] to fill the missing co-array elements, thereby enabling the co-prime array to effectively utilize all of the offered DOFs.

After obtaining the increased DOFs from these NLAs, DOA estimation can be performed mainly based on two methodologies: the subspace fitting and the sparsity recovery. For the former, a rank restoring method, such as the spatial smoothing [15,16] and the spatial smoothed matrix direct constructing [17], should be implemented prior to the application of MUSIC algorithm since the equivalent input sources are fully coherent. For the latter, DOAs are recovered by utilizing the sparsity property of the sources in

☆ This work was supported by China Scholarship Council under No. 201506030035.

* Corresponding author.
E-mail addresses: N1509412L@e.ntu.edu.sg (J. Liu), zhangym0726@163.com (Y. Zhang), eylu@ntu.edu.sg (Y. Lu), wangweijiang@bit.edu.cn (W. Wang).

http://dx.doi.org/10.1016/j.dsp.2016.12.002
1051-2004/

the spatial domain [18–20], where the problem of off-grid sources was discussed in [21,22], coherent sources in [23] and wide-band sources in [24].

Inspired by these methods and NLA geometries, two kinds of multi-level co-prime array geometries are proposed in this article for DOA estimation applications with a better angle-resolution. The prior co-prime array is mainly based on two-level geometry to generate a set of large consecutive lags in its virtual DCA (since the K-level geometry only obtains a slight improvement over the two level one). Then, the enhancement of corresponding virtual aperture obeys the second power law (from $O(N)$ to $O(N^2)$). Our proposed K-level geometries are more flexible consisting of more than two levels (i.e. K-level), therefore the enhancement of virtual aperture obeys the Kth power law (from $O(N)$ to $O(N^K)$). Obviously, the K-level geometries can provide a more efficient way for improving the aperture as well as the angle-resolution. By vectorizing the covariance matrix of measurements from the K-level array, a class of virtual sparse ULAs with different angle-resolutions and different inter-element spacing are generated (called multi-resolution difference co-arrays). Then a class of DOA estimation with different angle-resolutions and scanning spaces can be performed based on such MRDCAs, thereby enabling the effective utilization of both the offered DOFs and the increased aperture. In a sense, the multi-resolution concept had been introduced to digital beam-forming with high angle-resolution in our prior work [25,26]. Here for DOA estimation object, one need to find the genuine DOAs and exclude the replica ones, therefore, a novel probability decision strategy is proposed by combining the results of multi-level DOA estimation.

The article is organized as follows. In Section 2, we review the virtual array signal model and establish some important theorems and properties about the angle-resolution of sparse ULA. In Section 3, the formation of two kinds of K-level co-prime arrays and their corresponding configurations of MRDCAs are derived. Section 4 presents the multi-resolution DOA estimation algorithm and the followed probability decision strategy. In Section 5, the simulation results are provided to numerically validate the method. Section 6 concludes this paper.

The following notations are used throughout: We use lowercase bold characters to denote vectors (e.g. $\mathbf{a}$), upper-case bold for matrices (e.g. $\mathbf{A}$) and upper-case outline for a set (e.g. $\mathbb{A}$). For a matrix $\mathbf{A}$, the symbols $\mathbf{A}^*$, $\mathbf{A}^T$ and $\mathbf{A}^H$ denote the conjugation, transpose and conjugate transpose, respectively. $diag\{\mathbf{A}\}$ denotes a column vector consisting of the main diagonal elements of matrix $\mathbf{A}$. $diag\{\mathbf{a}\}$ denotes a diagonal matrix that uses the elements of vector $\mathbf{a}$ as its diagonal elements. $vec\{\mathbf{A}\}$ denotes vectorization, which converts the matrix $\mathbf{A}$ into a column vector by stacking the columns of the matrix $\mathbf{A}$ on top of one another. The symbols $\odot$ and $\otimes$ respectively denote the Khatri–Rao product and Kronecker product between two matrices of appropriate size, respectively. The symbol $\mathbb{Z}$ denotes the set of all integers. The symbol $\mathbb{Z}_a^b$ $(a \le b)$ denotes the set consisting of integers from a to b, $\mathbb{Z}_a^b \triangleq \{a, a+1, \ldots, b\}$. $gcd(\bullet)$ denotes the greatest common divisor.

2. Signal model and problem formulation

2.1. Definition

Definition 1 *(Set operation).* For any two sets of integers $\mathbb{A}$ and $\mathbb{B}$, one can define the following operations:

Intersection Set: $\mathbb{A} \cap \mathbb{B} = \{a : \forall a \in \mathbb{A} \text{ and } a \in \mathbb{B}\}$
Union Set: $\mathbb{A} \cup \mathbb{B} = \{a : \forall a \in \mathbb{A} \text{ or } a \in \mathbb{B}\}$
Sum Set: $\mathbb{A} + \mathbb{B} = \{a + b : \forall a \in \mathbb{A}, \forall b \in \mathbb{B}\}$
Difference Set: $\mathbb{A} - \mathbb{B} = \{a - b : \forall a \in \mathbb{A}, \forall b \in \mathbb{B}\}$
Translation Set: $\lambda + \mathbb{A} = \{\lambda + a : \forall a \in \mathbb{A}, \lambda \in \mathbb{Z}\}$
Dilation Set: $\lambda\mathbb{A} = \{\lambda a : \forall a \in \mathbb{A}, \lambda \in \mathbb{Z}\}$

Definition 2 *(Difference co-array of linear arrays [7]).* Considering a linear array of M sensors located at $\mathbb{A} = \{a_1, a_2, \ldots, a_N\}d_0$, where $a_i d_0$ denotes the ith sensor position, the difference co-array of the given array is defined as the array of sensors located at $\mathbb{D}$, where $\mathbb{D} \triangleq \mathbb{A} - \mathbb{A}$.

In the prior DCA model, a virtual ULA with a minimal inter-element spacing d_0 and without holes is desirable for spatial sampling purpose. In this article, we further develop this notion into the multi-resolution difference co-array (MRDCA) perspective by considering a set of virtual ULAs with different inter-element spacing. Specifically, the MRDCA $\mathbb{R}(\alpha, \mathrm{L}_\alpha)$ is a virtual ULA contained in the difference co-array of the given array and with inter-element spacing αd_0 up to one-sided aperture $\alpha d_0 L_\alpha$. Therefore, in mathematical formulation, $\mathbb{R}(\alpha, \mathrm{L}_\alpha) \triangleq \alpha d_0 \mathbb{Z}_{-\mathrm{L}_\alpha}^{+\mathrm{L}_\alpha} \subseteq \mathbb{D}$.

2.2. Review of DOA estimation based on DCA

Considering that a non-uniform linear array with M sensors at locations $\mathbb{A} = \{l_1, l_2, \cdots, l_{\mathrm{M}}\}$ in units of half a minimal wavelength in space and D far-field narrowband sources impinges to the array from directions θ_i, $i = 1, 2, \cdots, D$, therefore the array output can be expressed as (1):

$$\mathbf{x}(n) = \sum_{k=1}^{D} \mathbf{a}(\theta_k) s_k(n) + \mathbf{w}(n) = \mathbf{A}(\theta) s(n) + \mathbf{w}(n) \tag{1}$$

where $\mathbf{w}(n)$ denotes zero-mean and statistically independent additive Gaussian white noise. $\mathbf{A} = [\mathbf{a}(\theta_1), \mathbf{a}(\theta_2), \ldots, \mathbf{a}(\theta_D)]$ is the $M \times D$ array manifold matrix, whose kth column is the steering vector $\mathbf{a}(\theta_k)$ corresponding to the kth DOA. The mth element of $\mathbf{a}(\theta_k)$ is defined as $\mathbf{a}_m(\theta_k)$ (where $\mathbf{a}_m(\theta_k) = e^{j2\pi l_m v(\theta_k)}$ and $v(\theta_k) = \frac{d_0}{\lambda}\sin(\theta_k)$). Then the covariance matrix can be formed by (2):

$$\mathbf{R}_{xx} = E[\mathbf{x}\mathbf{x}^H] = \mathbf{A}(\theta)\mathbf{R}_{ss}\mathbf{A}(\theta)^H + \sigma_n^2 \mathbf{I}_M \tag{2}$$

Based on difference co-array perspective [7], the covariance matrix in (2) can be directly vectorized into an $M^2 \times 1$ vector:

$$\begin{aligned} \mathbf{z} &= vec(\mathbf{R}_{xx}) \in \mathbb{C}^{M^2 \times 1} \\ &= (\mathbf{A}^*(\theta) \odot \mathbf{A}(\theta))\mathbf{p} + \sigma_n^2\, vec\{\mathbf{I}_M\} \\ &= \hat{\mathbf{A}}(\theta)\mathbf{p} + \sigma_n^2 \mathbf{l}_M \end{aligned} \tag{3}$$

where $\mathbf{p} = diag\{\mathbf{R}_{ss}\}$ and $\mathbf{l}_M = vec\{\mathbf{I}_M\}$.

By comparing (3) and (1), one can find that $\mathbf{z}$ behaves like a single-snapshot output signal from an array with sensors at locations $(\mathbb{A} - \mathbb{A})$. $\mathbf{p}$ and $\mathbf{l}_M$ are equivalent input sources and noise. $\hat{\mathbf{A}}$ is an augmented array manifold. Therefore, DOA estimation can be performed based on the virtual array model (3) rather than the physical array model (1). For this purpose, there are two main methodologies: the sparsity recovery and the subspace fitting (SSF). Here we mainly focus on SSF method (more practical and more effective for engineering purpose), it proceeds as follows. The SSF method requires consecutive virtual sensor positions, therefore, one can select a uniform linear difference co-array with a minimal inter-element spacing, denoted as $\mathbb{R}(1, L_1)$. The NLA signal model (3) can be reduced into a ULA signal model (4):

$$\mathbf{z}_1 = \hat{\mathbf{A}}_1(\theta)\mathbf{p} + \sigma_n^2 \mathbf{e}_{L_1} \in \mathbb{C}^{(2L_1+1)\times 1} \tag{4}$$

where $\mathbf{e}_{L_1} = \begin{bmatrix}\mathbf{0}_{1\times L_1} & 1 & \mathbf{0}_{1\times L_1}\end{bmatrix}^T$. Compared to the conventional physical array model, two points should be specially noted: firstly, there is only one non-zero element in $\mathbf{e}_{L_1}$, which indicates that the noise only affects the zero-lag virtual sensor. The corresponding influence can be canceled out by applying a noise power suppression to the output of the zero-lag sensor or by adopting a general algorithm for DOA estimation in the presence of non-uniform

noise [27]. Secondly, the single snapshot virtual input source vector $\mathbf{p}$ is fully coherent, therefore, a rank restoring method should be implemented prior to the application of DOA algorithm. In this article, the forward spatial smoothing [15] MUSIC algorithm is applied to the measurement vector $\mathbf{z}_1$ without any non-uniform noise processing. The spatial smoothed covariance matrix can be formed by (5):

$$\mathbf{R}_{z_1 z_1} = \sum_{\ell=1}^{L_1} \mathbf{S}_\ell \mathbf{z}_1 \mathbf{z}_1{}^H \mathbf{S}_\ell^H \in \mathbb{C}^{(L_1+1)\times(L_1+1)} \tag{5}$$

where $\mathbf{S}_\ell = \left[\mathbf{0}_{(L_1+1)\times(\ell-1)} \;\; \mathbf{I}_{(L_1+1)} \;\; \mathbf{0}_{(L_1+1)\times(L_1+1-\ell)}\right]$ denotes the selection matrix. The MUSIC spectra $\mathbf{P}_{z_1}(\dot{\theta})$ can be calculated by (6):

$$\mathbf{P}_{z_1}(\dot{\theta}) = \frac{1}{\|\mathbf{a}(\dot{\theta})^H \mathbf{v}_n\|^2} \quad \forall\ \dot{\theta} \in \mathbf{\Theta} \tag{6}$$

where $\mathbf{v}_n$ is the eigenvector of noise space obtained by performing eigenvalue decomposition of the rank restored covariance matrix $\mathbf{R}_{z_1 z_1}$, $\dot{\theta}$ denotes the potential DOA in a certain scanning grid space. In this article, we define a kind of non-uniform scanning grid space Θ as (7), where the corresponding $v(\dot{\theta}_i)$ is uniformly distributed from -0.5 to 0.5 with a grid interval of $\frac{1}{2N}$.

$$\begin{cases} \text{GridSpace:} & \mathbf{\Theta} \triangleq [\dot{\theta}_{-N} \sim \dot{\theta}_N] \\ \text{GridInterval:} & \Delta \triangleq \|v(\dot{\theta}_{i+1}) - v(\dot{\theta}_i)\| = \frac{1}{2N} \end{cases} \tag{7}$$

The following conclusions can be drawn: on the capacity, the dimension of spatial smoothed matrix is $(L_1+1)\times(L_1+1)$, therefore, the maximum number of resolvable sources is L_1. On the resolution, for simplicity, considering two plane waves with spatial frequency separation $\triangle_\theta$ impinging on a MRDCA $\mathbb{R}(d_1, L_1)$ (which behaves like a ULA consisting of $2L_1+1$ sensors with inter-element spacing being $d_1 d_0$), the resolution of MUSIC algorithm has been proved in [28] and can be expressed as (8):

$$\Upsilon_{\text{MUSIC}}(\triangle_\theta) = 1 - \frac{2f^2(z/2)}{1+|f(z)|} \tag{8}$$

where $f(z) = \frac{\sin(\pi(2L_1+1)d_1 d_0 \triangle_\theta)}{(2L_1+1)\sin(\pi d_1 d_0 \triangle_\theta)}$ and $z = \pi(2L_1+1)d_1 d_0 \triangle_\theta$. The two plane waves are resolved if $\Upsilon_{\text{MUSIC}}(\triangle_\theta) > 0$. There are two strategies to improve the angle-resolution in (8): increasing the element number L_1 or increasing the inter-element spacing d_1. For the former, one needs to operate a large-scale array with massive sensors and to search in the full space range with a small grid interval. These two operations would result in formidable system complexity and costs. Therefore, as an effective way to increase the angle-resolution, a multi-resolution DOA estimation method is proposed by nesting several virtual ULAs with different inter-element spacings.

2.3. MRDCA and spatial aliasing

As we know, the array-based spatially sampling in DOA estimation system is similar to the time-based sampling in temporal system. Just as there is a Nyquist sampling rate in temporal processing, there is a maximum inter-element spacing $\lambda/2$ in spatial processing. If the inter-element spacing of the physical array is larger than $\lambda/2$, the DOAs of the sources are not able to resolve uniquely, resulting in spatial aliasing [29]. Specifically, the fundamental reason for this phenomenon is that two different DOAs (i.e. θ_i and θ_j) produce the same steering vector, as expressed in (9):

$$\begin{aligned} e^{-2j\pi d v(\theta_i)} &= e^{-2j\pi d v(\theta_j)} \\ \mathbf{a}(\theta_i) &= \mathbf{a}(\theta_j) \end{aligned} \tag{9}$$

For example, a narrowband signal impinges on three kinds of uniform arrays consisting of 8 sensors with different inter-element spacing ($d = \lambda/2, \lambda, 2\lambda$) from direction $\theta_4 = 45°$. The corresponding spectra are illustrated in Fig. 1. In-depth comparisons and analyses are performed as the following two aspects:

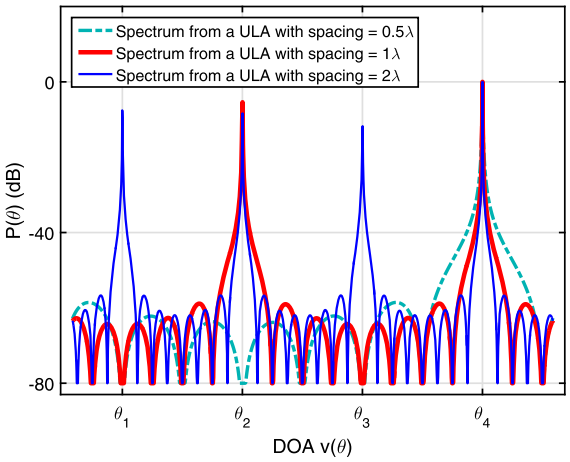

Fig. 1. Comparisons of the MUSIC spectra of three kinds of uniform linear arrays with inter-element spacing being $\frac{\lambda}{2}$, λ, 2λ, where the genuine DOA arrivals from direction $\theta_4 = 45°$.

- On the number of ambiguous DOAs: for the array with $d = \lambda/2$, an unique genuine DOA can be detected. For the array with $d = \lambda$, two DOAs can be detected including a genuine DOA and a replica. For the array with $d = 2\lambda$, four DOAs can be detected, including a genuine DOA and three replicas.
- On the resolution: as expected, the array with larger inter-element spacing possesses a larger physical aperture and accordingly achieves a higher resolution.

As a conclusion, a theorem about the spatial aliasing of MRDCA is provided as

Theorem 1. *Assume that a narrowband signal impinges on an MRDCA $\mathbb{R}(k, L_k)$ from direction θ_0, then, as many as $(k-1)$ distinct replicas $s\{\hat{\theta}_1, \hat{\theta}_2, \ldots, \hat{\theta}_{k-1}\}$ can be generated in the full space range from $-90°$ to $90°$.*

Proof. Assume that the genuine DOA is θ_0 and any one of the replicas is $\hat{\theta}_i$, where both $\hat{\theta}_i$ and θ_0 belong to $[-90°, 90°]$. Based on the constraint criterion in (9), one can obtain (10):

$$e^{-j2\pi k v(\theta_0)} = e^{-j2\pi k v(\hat{\theta}_i)} \tag{10}$$

As we know, the complex exponential function, $f_k(t) = e^{-j2\pi kt}$, is a periodic function with minimum positive period $T_{\min}(k) = 1/k$. Therefore the unified solution for (10) can be expressed as (11):

$$v(\hat{\theta}_i) = v(\theta_0) + \ell T_{\min}(k), \quad \ell \in \mathbb{Z} \tag{11}$$

where ℓ can be any integer. Consider the constraint $\hat{\theta}_i \in [-90°, 90°]$, then $v(\hat{\theta}_i) \in [-\frac{d_0}{\lambda}, \frac{d_0}{\lambda}] = [0.5, 0.5]$. Therefore the total number of solutions for equation (11) is $1/T_{\min}(k) = k$. Obviously, it should include a genuine DOA θ_0 and $(k-1)$ distinct replicas $\{\hat{\theta}_1, \hat{\theta}_2, \ldots, \hat{\theta}_{k-1}\}$. □

Theorem 1 implies that the MRDCA can result in ambiguous DOAs. This phenomenon can also be further utilized to reduce the scanning grid space as well as improve angle-resolution. Therefore, let us directly introduce the following Corollary 1.

Corollary 1. *In a narrowband DOA estimation system based on the MRDCA $\mathbb{R}(k, L_k)$, the scanning space range can be reduced into (12). In*

addition, the MUSIC spectra of the full space range $\mathbf{P}_{z_1}(\boldsymbol{\Theta})$ *can be recovered by replicating the spectra of the reduced space range* $\mathbf{P}_{z_1}(\boldsymbol{\Theta}_k)$ *based on (13):*

$$\begin{cases} \text{ReducedGridSpace:} & \boldsymbol{\Theta}_k = [\dot{\theta}_{\frac{-N}{k}} \sim \dot{\theta}_{\frac{N}{k}}] \\ \text{ImprovedGridInterval:} & \triangle_k = \frac{1}{2kN} \end{cases} \tag{12}$$

$$\mathbf{P}_{z_1}(\dot{\theta}_i) = \mathbf{P}_{z_1}(\dot{\theta}_{i+\frac{2N\ell}{k}}) \; \forall \, \dot{\theta}_i \in \boldsymbol{\Theta}_k, \; \dot{\theta}_{i+\frac{2N\ell}{k}} \in \boldsymbol{\Theta}, \ell \in \mathbb{Z} \tag{13}$$

Corollary 1 implies that, by making using of the spatial aliasing, the independent searching times is always $2N$ no matter what kind of MRDCA configuration one chooses. In practice, take a very limited number of combinations of levels into consideration, the linear increased searching times is still more effective, compared to the huge searching times in the full space range.

3. Multi-level generalized co-prime arrays

Co-prime array [7] and nested array [8] mainly consisted of two overlapped sparse ULAs with different inter-element spacings. Such two-level geometries had been deeply researched due to their abilities to enhance DOFs. The author in [11] generalized the co-prime array configuration with two operations. The first one was the compression of the inter-element spacing of one subarray, which made the nested array become the special case of the co-prime array. The second one was the displacement of two subarrays, which made the minimum inter-element spacing much larger than the half-wavelength. The resulting co-array geometries are referred as co-prime array with compressed inter-element spacing (CACIS) and co-prime array with displaced subarrays (CADiS). Their physical array formations and consecutive virtual array configurations[1] are expressed as (14):

$$\begin{cases} \mathbb{P}_{\text{CACIS}} = M_1\mathbb{Z}_0^{M_2-1} \bigcup \dot{M}_2\mathbb{Z}_0^{M_1-1} \\ \mathbb{V}_{\text{CACIS}} = \mathbb{Z}_{-L_{\text{CACIS}}}^{+L_{\text{CACIS}}} \\ \mathbb{P}_{\text{CADiS}} = M_1\mathbb{Z}_0^{M_2-1} \bigcup \left(\dot{M}_2\mathbb{Z}_0^{M_1-1} + L_{\text{opt}}\right) \\ \mathbb{V}_{\text{CADiS}} = \mathbb{Z}_{-L_{\text{CADiS}}}^{+L_{\text{CADiS}}} \end{cases} \tag{14}$$

where $gcd(M_1, M2) = 1$, $M_1 > M_2$, $M_2 = p\dot{M}_2$, $L_{\text{opt}} = M_1(M_2 - 1) + M_1 + 1$, $L_{\text{CACIS}} = M_1M_2 - \dot{M}_2(M_1 - 1) - 1$, $L_{\text{CADiS}} = M_1M_2$.

Inspired by aforementioned array geometries and considering a more flexible array configurations with more than two levels (i.e. K-level), then, we present two kinds of K-level generalized co-prime arrays. Compared to the two-level ones, the K-level arrays have the potential to generate many MRDCAs with different levels of angle-resolution. Both the formation of the arrays and the corresponding properties are presented in the following sequel, and the multi-resolution estimation algorithm is presented in Section 4.

3.1. K-level overlapped co-prime array

The first K-level array geometry consists of K overlapped ULAs with different inter-element spacings, as shown in Fig. 2. Assuming that the nth level subarray (where $1 \le n \le K$) consists of K_n sensors with inter-element spacing being d_nd_0 and the first sensor is shared by all the sub-arrays, it is called K-level overlapped co-prime (K-OveCoprime) array whose element positions can be described by a set of positive integers $\{(K_1, d_1), (K_2, d_2), \ldots, (K_k, d_k)\}$. Specifically, choosing the first element as a reference, the element positions of nth level can be expressed as (15):

[1] All the element positions are in unit of a minimal inter-element spacing d_0 in the sequel.

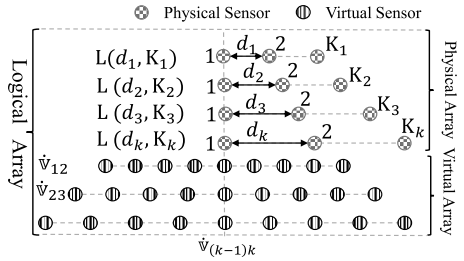

Fig. 2. The K-level overlapped co-prime array geometry $\mathbf{L}(d_n, K_n)$, $n = 1, \cdots, K$, and the corresponding multi-level virtual arrays $\dot{\mathbb{V}}_{\text{mn}}$.

Table 1
A numerical example of a K-OveCoprime array configuration.

Physical	K_n	d_n	$\dot{\mathbb{P}}_n$
1st	7	3	{0, 3, 6, 9, 12, 15, 18}
2nd	6	7	{0, 7, 14, 21, 28, 35}
3th	7	21	{0, 21, 42, 63, 84, 105}
4th	6	42	{0, 42, 84, 126, 168, 210}
Virtual	**DOF$_n$**	**d_{mn}**	**$\dot{\mathbb{V}}_{\text{mn}}$**
L_{12}	47	1	$\{-23, -22, \ldots, 22, 23\}$
L_{13}	71	3	$\{-35, -34, \ldots, 34, 35\} \times 3$
L_{24}	61	7	$\{-30, -29, \ldots, 29, 30\} \times 7$

$$\dot{\mathbb{P}}_n = d_n\mathbb{Z}_0^{K_n-1} \tag{15}$$

Then, taking all the K levels into consideration, the element positions can be expressed as (16):

$$\mathbb{P}_{\text{O}}(K_1, K_2, \ldots, K_k) = \bigcup_{n=1}^{K} \left(d_n\mathbb{Z}_0^{K_n-1}\right) \tag{16}$$

It is noted that, as a special case, when choosing $d_1 = 1$, $d_k = \prod_{n=1}^{k-1}\{K_n\}$, the proposed K-level co-prime array becomes a K-level nested array [7]. Then, much attention would be focused on the virtual array generated by above K-level physical array. Ideally, we hope that the DCAs of the proposed K-level co-prime array has no holes so that DOFs can be significantly increased. Unfortunately, only a slight improvement is achieved, compared to the two level one. Therefore, we propose a new perspective by dividing the virtual array into a set of MRDCAs enabling the utilization of both the increased DOFs and the enlarged virtual aperture. For example, consider a pair of sub-arrays, (i.e. the mth and the nth), their difference co-array can be expressed as (17):

$$\begin{aligned} \dot{\mathbb{P}}_{\text{mn}} &= \dot{\mathbb{P}}_n \cup \dot{\mathbb{P}}_m = \left(d_n\mathbb{Z}_0^{K_n-1} \cup d_m\mathbb{Z}_0^{K_m-1}\right) \\ &= \underbrace{\left(a_n\mathbb{Z}_0^{K_n-1} \cup a_m\mathbb{Z}_0^{K_m-1}\right)}_{\text{CACIS}} d_{\text{mn}} \\ \dot{\mathbb{V}}_{\text{mn}} &\supseteq \mathbb{R}(d_{\text{mn}}, L_{\text{mn}}) \end{aligned} \tag{17}$$

where $d_{\text{mn}} = gcd(d_m, d_n)$. Since a_n and a_m are co-prime integers, $(a_n\mathbb{Z}_0^{K_n-1} - a_m\mathbb{Z}_0^{K_m-1})$ can behave like a CACIS in (14) by appropriate choosing $K_n = a_m$ and $K_m = a_np$. (17) indicates that an MRDCA $\mathbb{R}(d_{\text{mn}}, L_{\text{mn}})$ is contained in the virtual array $\dot{\mathbb{V}}_{\text{mn}}$.

As a numerical example, Table 1 lists all the configurations of a four-level overlapped co-prime array. This four level OveCoprime array consists of only 19 physical sensors, while its physical aperture is as large as $210d_0$. The first virtual array of interest is L_{12}, as MRDCA $\mathbb{R}(1, 23)$, which consists of 47 virtual sensors with a unit inter-element spacing. The second one is L_{13}, as MRDCA $\mathbb{R}(3, 35)$, which consists of 71 virtual sensors with three times inter-element spacing. The third is L_{24}, as MRDCA $\mathbb{R}(7, 30)$, which consists of 61 virtual sensors with seven times inter-element spacing.

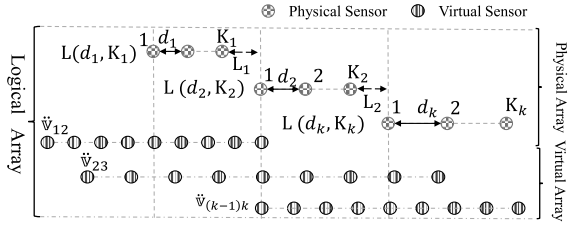

Fig. 3. The K-level displaced co-prime array geometry $\mathbf{L}(d_n, K_n)$, $n = 1, \cdots, K$, and the corresponding multi-level virtual arrays $\ddot{\mathbb{V}}_{\mathrm{mn}}$.

3.2. K-level displaced co-prime array

For the K-OveCoprime array, all of its sub-arrays are overlapped. By introducing a appropriate displacement among the subarrays, the second kind of K-level geometries called K-level Displaced Co-prime (K-DisCoprime) array is proposed, as shown in Fig. 3. Compared to the K-OveCoprime array, both the physical aperture and the inter-element spacing are enlarged for the K-DisCoprime array. Assume that the nth level sub-array (where $1 \le n \le K$) consists of K_n sensors with inter-element spacing being $d_n d_0$. However there is a displacement L_n for the two adjacent sub-arrays (i.e. nth and $(n+1)$th). Therefore, this geometry can also be described by a set of positive integers $\{(K_1, d_1, L_1), (K_2, d_2, L_2), \ldots, (K_k, d_k, L_k)\}$. Choosing the first element as a reference, the element positions of nth level can be expressed as (18):

$$\ddot{\mathbb{P}}_n = \Gamma_n + d_n \mathbb{Z}_0^{K_n - 1} \tag{18}$$

where $\Gamma_n = \sum_{i=1}^{n-1} \{L_i + d_i(K_i - 1)\}$. According to [11], the optimal displacement L_i can be chosen as $L_i = (K_i + 1)d_i$. Then, all the element positions of the K-DisCoprime array can be expressed as (19):

$$\mathbb{P}_{\mathrm{D}}(K_1, K_2, \ldots, K_k) = \bigcup_{n=1}^{K} \left(\Gamma_n + d_n \mathbb{Z}_0^{K_n - 1} \right) \tag{19}$$

Then we focus on the virtual array generated by a pair of adjacent sub-arrays (i.e. the mth and the nth, where $m = n + 1$). The difference co-array can be expressed as (20):

$$\begin{aligned} \ddot{\mathbb{P}}_{\mathrm{mn}} &= \ddot{\mathbb{P}}_n \cup \ddot{\mathbb{P}}_m = (d_n \mathbb{Z}_0^{K_n - 1} + \Gamma_n) \cup (d_m \mathbb{Z}_0^{K_m - 1} + \Gamma_m) \\ &= d_n \mathbb{Z}_0^{K_n - 1} \cup (d_m \mathbb{Z}_0^{K_m - 1} + \Gamma_m - \Gamma_n) \\ &= \underbrace{\left(a_n \mathbb{Z}_0^{K_n - 1} \cup (a_m \mathbb{Z}_0^{K_m - 1} + \ddot{L}_{\mathrm{mn}}) \right)}_{\text{CADiS}} d_{\mathrm{mn}} \\ \ddot{\mathbb{V}}_{\mathrm{mn}} &\supseteq \mathbb{R}(d_{\mathrm{mn}}, L_{\mathrm{mn}}) \end{aligned} \tag{20}$$

Since a_n and a_m are co-prime integers, $\left(a_n \mathbb{Z}_0^{K_n - 1} \cup (a_m \mathbb{Z}_0^{K_m - 1} + \ddot{L}_{\mathrm{mn}}) \right)$ could convert into a CADiS in (14) by appropriately choosing $K_n = a_m$ and $K_m = a_n p$. In addition, (20) also indicates that an MRDCA $\mathbb{R}(d_{\mathrm{mn}}, L_{\mathrm{mn}})$ is contained in the virtual array $\ddot{\mathbb{V}}_{\mathrm{mn}}$. As a numerical example, Table 2 lists all the configurations of a three-level displaced co-prime array. This three level DisCoprime array consists of only 21 physical sensors, while its physical aperture is as large as $406d_0$. The first virtual array of interest is L_{12}, as MRDCA $\mathbb{R}(1, 56)$. The second one is L_{23}, as MRDCA $\mathbb{R}(7, 56)$.

Above analyses and numerical results validate that the proposed K-level co-prime arrays can significantly increase the array aperture and generate many MRDCAs. According to the Corollary 1, their corresponding scanning space can be reduced, respectively. In Section 4, we focus on how to achieve high angle-resolution DOA estimation based on these generated MRDCAs.

Table 2
A numerical example of a K-DisCoprime array configuration.

Physical	K_n	d_n	L_n	$\ddot{\mathbb{P}}_n$
1st	7	1	8	{0, 1, 2, 3, 4, 5, 6}
2nd	7	7	56	{14, 21, 28, 35, 42, 49, 56}
3th	7	49	112	{112, 161, 210, 259, 308, 357, 406}
Virtual	**DOF$_n$**	**d_{mn}**		**$\ddot{\mathbb{V}}_{\mathrm{mn}}$**
L_{12}	113	1		$\{-56, -55, \ldots, 55, 56\}$
L_{23}	113	7		$\{-56, -55, \ldots, 55, 56\} \times 7$

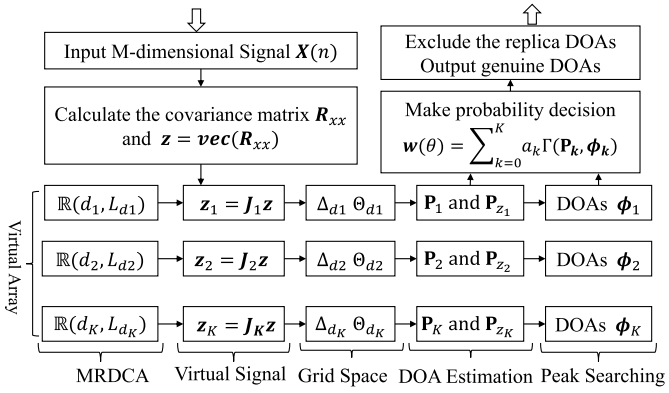

Fig. 4. The procedure of multi-resolution DOA estimation based on the K-level co-prime array.

4. Multi-resolution DOA estimation algorithm

After obtaining the reduced scanning space, DOA estimation can be preformed directly based on (6) in each level. As a result, all the genuine DOAs as well as replica ones can be detected with different resolutions, where the number of replicas is $(d_{\mathrm{mn}} - 1)$ times that of the genuine ones. Therefore, the overall procedure, as shown in Fig. 4, can be divided into two main sub-procedures: the multi-resolution DOA (MR-DOA) estimation and the probability decision.

4.1. Multi-resolution DOA estimation

Considering a multi-level co-prime array of M sensors, the covariance matrix $\mathbf{R}_{xx}$ in (2) can be vectorlized into an $M^2 \times 1$ virtual signal. For the kth level MRDCA of interest, as $\mathbb{R}(d_k, L_{d_k})$, where $1 \le k \le K$, $(2L_{d_k} + 1)$ sensors can be selected from M^2 virtual sensors by (21):

$$\mathbf{z}_k = \mathbf{J}_k \, vec(\mathbf{R}_{xx}) \tag{21}$$

where $\mathbf{J}_k$ is a $(2L_{d_k} + 1) \times M^2$ selection matrix. There is only one non-zero element in each row, whose location is corresponding to the index of the selected virtual element among M^2 virtual sensors.

For each level virtual array, the potential DOAs can be estimated by using MUSIC algorithm in (6) from the reduced scanning space in (12). According to Theorem 1 and (13), the spectra and DOAs for the full space range can be obtained by directly replicating. Therefore, the steps of MR-DOA estimation are summarized in Algorithm 1.

4.2. Probability decision

All the ambiguous DOAs have been obtained by above MR-DOA algorithm. According to Theorem 1, only part of them are genuine DOAs, while others are replicas. Therefore, much attention should be focused on how to identify the genuine ones and exclude the

Algorithm 1 The MR-DOA estimation.

Input: M-dimensional observations $\mathbf{X}(n)$.
Output: The estimated multi-resolution spectra: $\mathbf{P}_k(\theta)$ and DOAs: $\emptyset_k(\theta)$ for $k = 1, 2, \ldots, K$.
Initialize: Set $k = 1$.

1: Calculate the covariance matrix $\mathbf{R}_{xx}$ by (2).
2: Repeat
3: Select the kth MRDCA $\mathbb{R}(d_k, L_{d_k})$ based on (17) and (20);
Form the kth virtual signal $\mathbf{z}_k$ based on (21);
Establish the kth grid space $\mathbf{\Theta}_{d_k}$ and $\mathbf{\Delta}_{d_k}$ based on (12).
4: Obtain the spectrum of sub-grid $\mathbf{P}_{z_k}(\dot{\theta})$, where $\dot{\theta} \in \mathbf{\Theta}_{d_k}$, based on (4)–(6): $\mathbf{z}_k \Rightarrow \mathbf{R}_{z_k z_k} \Rightarrow \mathbf{P}_{z_k}(\dot{\theta})$.
5: Obtain the spectrum of full-grid $\mathbf{P}_{z_k}(\theta)$, where $\theta \in \mathbf{\Theta}$, based on Theorem 1 and (13): $\mathbf{P}_k(\theta) = \mathbf{P}_{z_k}(\theta)$.
6: Find all the DOAs $\emptyset_k$ by searching peak point of $\mathbf{P}_k$.
7: Set $k = k + 1$.
8: Until $k > K$.
9: Output the estimated results: $\mathbf{P}_k(\theta)$ and $\emptyset_k(\theta)$.

replicas. For this purpose, the prior work, such as a compressed searching method [29] and a projection method [30], were mainly based on a simple binary decision strategy. In this article, we propose a probability-based decision strategy. Specifically, for all the scanning angle θ, a probability function $w(\theta)$ can be estimated, whose value reflects the probability of existing a target at specific angle, where $0 \le w(\theta) \le 100\%$. Then, the final decision can be made based on probability criterion with a threshold ρ.

$$\begin{cases} w(\theta) \ge \rho, & \text{Target exists with probability } \rho \\ w(\theta) < \rho, & \text{Target does not exist with probability } \rho \end{cases} \tag{22}$$

The final probability function $w(\theta)$ should be calculated by combining both the DOA peak $\emptyset_k$ and the pseudo spectrum $\mathbf{P}_k(\theta)$ of the different levels. Furthermore, there are some basic facts to obtain the specific criterions of the probability function.

- The genuine peak position is independent on the sparse inter-element spacing, while the replicate peak position is highly dependent on it.
- As the increasing of the virtual array aperture, the peak becomes much thinner and much sharper.
- As the increasing of the inter-element spacing, the much more number of replicas are generated, which lead to a certain loss of credibility for the peak being a genuine DOA.

According to these facts, the criterion of probability function can be defined as (23) by introducing an abstract operation named combine sum $\biguplus$.

$$w(\theta) = \biguplus_{k=1}^{K} \alpha_k w_k(\theta) = \biguplus_{k=1}^{K} \{\alpha_k \mathcal{F}_k(\mathbf{P}_k, \emptyset_k)\} \tag{23}$$

where α_k denotes a penalty factor and implies the weight percentage of kth level in the final decision. $w_k(\theta)$ denotes the probability function of kth level and is obtained as a result of a transform operation $\mathcal{F}_k(\cdot)$ to the DOA peak $\emptyset_k$ and the pseudo spectrum $\mathbf{P}_k(\theta)$.

Firstly, we focus on the probability function of a given level (i.e. kth). All the angles corresponding to peak positions should possess equivalent and maximum probability. It can be expressed as $\mathcal{F}_k(\theta_i) = 1$ for $\theta_i \in \emptyset_k$. However, for $\theta_i \notin \emptyset_k$, assuming that the closest peak position is $\hat{\theta}$, one can define a relative power attenuation of pseudo spectrum as $\triangle\mathbf{P}_k(\theta)$, $\triangle\mathbf{P}_k(\theta) = \mathbf{P}_k(\hat{\theta}) - \mathbf{P}_k(\theta) \ge 0$. For a angle θ and a cutoff threshold ξ_k, if the relative power attenuation $\triangle\mathbf{P}_k(\theta)$ is greater than the cutoff threshold ξ_k, we consider that no target impinge from this direction and the corresponding value of the probability function is 0. Therefore, the probability function $w_k(\theta)$ can be expressed as (24):

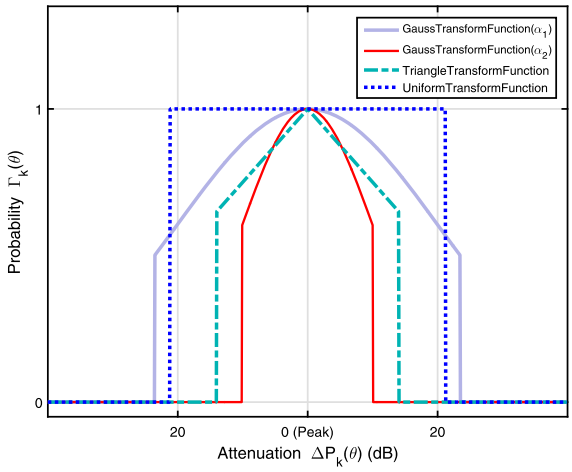

Fig. 5. The comparison of four kinds of transform functions.

$$w_k(\theta) = \begin{cases} 1 & \triangle\mathbf{P}_k(\theta) = 0 \\ 0 & \triangle\mathbf{P}_k(\theta) > \xi_k(\theta) \\ \mathcal{F}_k(\mathbf{P}_k, \emptyset_k) \in (0, 1) & \text{elsewhere} \end{cases} \tag{24}$$

According to above facts and criterions, three kinds of transform functions are proposed, as shown in Fig. 5. One can refer to Appendix A for their detailed mathematical expressions.

Secondly, we focus on final decision by combining the probability function of different level. As mentioned, for the peak of genuine DOA is independent on the sparse inter-element spacing. Therefore, for a potential angle θ, which belongs to $\emptyset_k$ for all the levels, a target arrivals from this direction with probability 1. The peak of the replica DOA only exists in some specific levels, therefore, the position will be considered as a replica one as long as $w_k(\theta)$ is 0 within a certain level, the corresponding probability function value $w(\theta)$ being 0. As a conclusion, the final probability function $w(\theta)$ can be expressed as (25):

$$w(\theta) = \biguplus_{k=1}^{K} \alpha_k w_k(\theta) = \begin{cases} 1 & \forall w_k(\theta) = 1 \\ 0 & \exists w_k(\theta) = 0 \\ \sum_{k=1}^{K} a_k w_k(\theta) & \forall w_k(\theta) \ne 0 \end{cases} \tag{25}$$

Thirdly, we focus on the penalty parameters a_k and the transform function $\mathcal{F}_k(\bullet)$. For a MRDCA $\mathbb{R}(d_m, L_{d_m})$, according to Theorem 1, as many as d_m peaks are generated. In other words, any angle θ corresponding to a peak is a genuine DOA with probability $\varrho_k = 1/d_k$. Therefore, a_k can be set as (26):

$$a_k = \frac{\varrho_k}{\sum_{n=1}^{K} \varrho_k} \tag{26}$$

As the increasing of the virtual array aperture, the peak of the spectrum becomes much thinner and much sharper. Therefore, for the small aperture MRDCA, one should choose a flat top transform function (e.g. rectangular transform function) with a relative loose threshold. For the large aperture MRDCA, one should choose a sharp-pointed transform function (e.g. triangle transform function) with a strict threshold.

In the end, we focus on the probability threshold ρ in (22), which has an important impact in the rightness and credibility of estimations. Generally, one of the virtual MRDCAs should be selected with an inter-element spacing being d_0 without generating spatial aliasing. Therefore, the worst case is that all the replicated peaks happen to appear in a false position. In order to successfully exclude such a worst case, the threshold could be set as (27):

$$\rho \ge 1 - \prod_{n=1}^{K} \varrho_n = 1 - \prod_{n=1}^{K} \frac{1}{d_n} \tag{27}$$

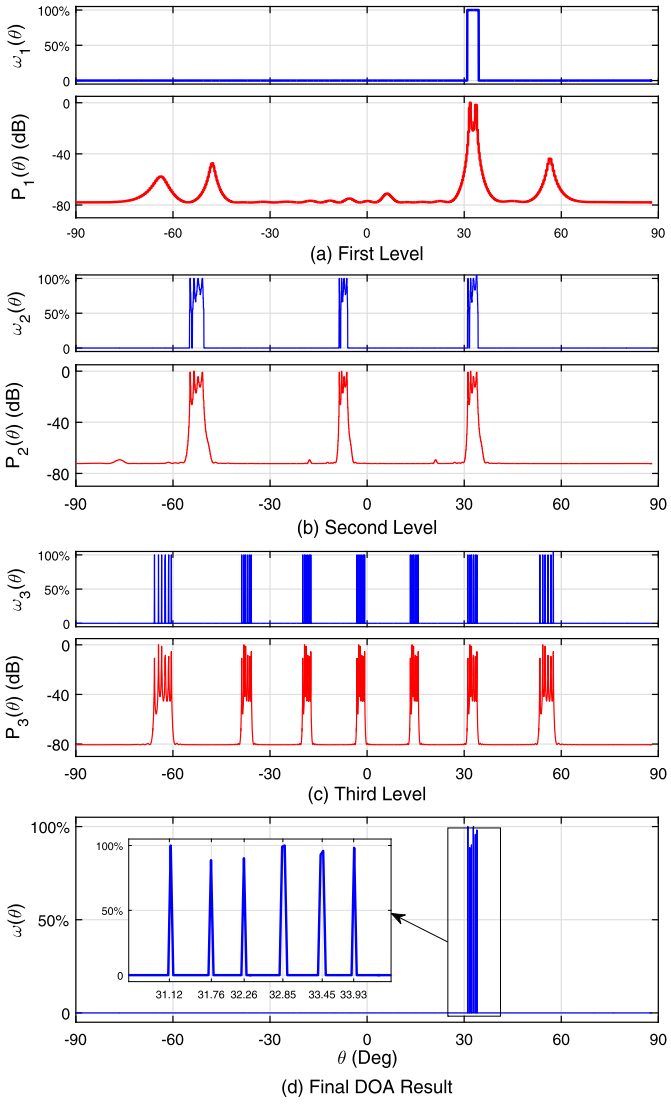

Fig. 6. The MUSIC spectra and corresponding probability functions based on a K-OveCoprime array by using the proposed MR-DOA algorithm and probability decision criterion: (a) the first level (b) the second level (c) the third level (d) the final estimated DOA results.

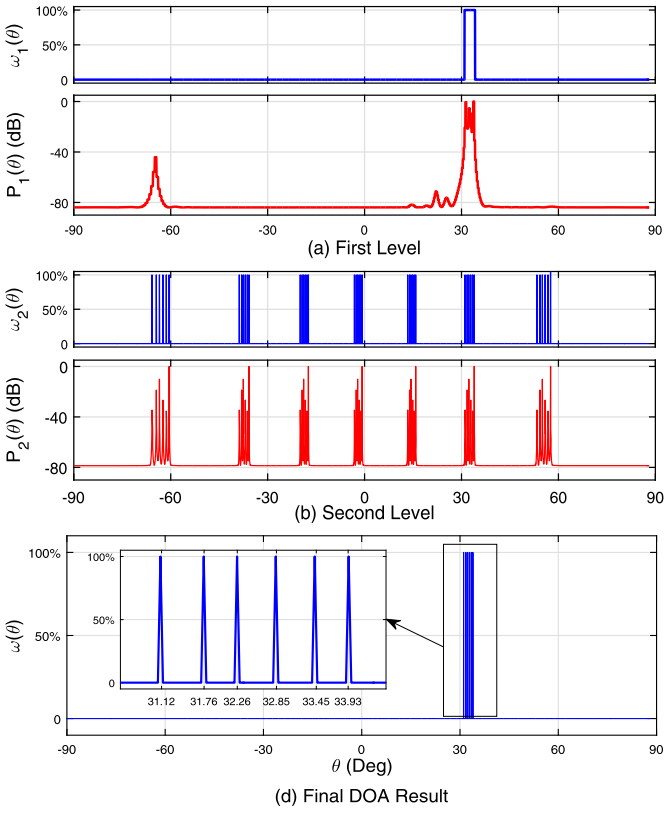

Fig. 7. The MUSIC spectra and corresponding probability functions based on a K-DisCoprime array by using the proposed MR-DOA algorithm and probability decision criterion: (a) the first level (b) the second level (c) the final estimated DOA results.

5. Numerical experiments and discussions

5.1. Performances of the proposed algorithms and arrays

In the first numerical experiment, the MR-DOA estimation is performed by using MUSIC algorithm based on the proposed two kinds of K-level co-prime arrays. The configurations of the physical and virtual sensors are listed in Table 1 and Table 2. Assuming that six close sources impinge from directions {31.12°, 31.76°, 32.26°, 32.85°, 33.45°, 33.93°}, 2000 snapshots with signal-to-noise ratio (SNR) being 10 dB are formed to estimate the covariance matrix.

For the K-OveCoprime array in Table 1, the virtual arrays of interest are L_{12}, L_{13} and L_{24}, whose properties have been discussed in Section 3. In order to perform MR-DOA estimation, for the first level, the rectangular transform function with $\xi_1 = 35$ dB is applied. For second and third levels, the triangle transform function with $\xi_2 = 25$, $\xi_3 = 15$ dB and $\rho_2 = 0.5$, $\rho_3 = 0.5$ are applied, respectively.

For the K-DisCoprime array in Table 2, the first virtual array of interest is L_{12} and the rectangular transform function with $\xi_1 = 35$ dB is applied. the second is L_{23} and the triangle transform function with $\xi_2 = 15$ dB and $\rho_2 = 0.5$ is applied. The MUSIC spectrum $\mathbf{P}_k(\theta)$ and the probability function $w_k(\theta)$ of each level are illustrated in Fig. 6 and Fig. 7.

For the K-OveCoprime array case, only two indistinct sources are detected due to the limited resolution in the first level. The corresponding probability function behaves like a rectangular function, which roughly forms the general outline of DOAs. In the second level, three groups of close sources are detected in the full range: one is genuine DOAs and the two others are replicas. In each group, as the improved resolution, four sources are detected and a more clear outline is formed by the corresponding probability function. In the third level, seven groups of close sources are detected: one genuine DOAs and six replica ones. Due to the super resolution resulted from the larger aperture, all the six sources are correctly and clearly detected via six sharp-pointed peaks.

For the K-DisCoprime array case, compared to the K-OveCoprime array, although much more virtual sensors are generated in its first level, only a slight improvement is obtained for such a case of close sources. Only three sources are detected and its probability function behaves like a rectangular function. The second level sub-array hosts a huge virtual aperture. As expected, all the close sources are correctly and clearly detected by six sharp-pointed peaks.

Based on the results of multi-level DOA estimation, one can perform final probability decision. For the K-OveCoprime array, the penalty factors are set as: $\alpha_1 = 21/31$, $\alpha_2 = 7/31$ and $\alpha_3 = 3/31$. For the K-DisCoprime array, $\alpha_1 = 7/8$ and $\alpha_2 = 1/8$. The final probability function $w(\theta)$ and its enlarged view are also illustrated in Fig. 6(d) and Fig. 7(c). It shows that all the replicas are successfully excluded by utilizing the proposed probability criterions. From the enlarged sub-figures, all the six genuine DOAs (represented by the vectorized grid lines) are clearly and correctly detected.

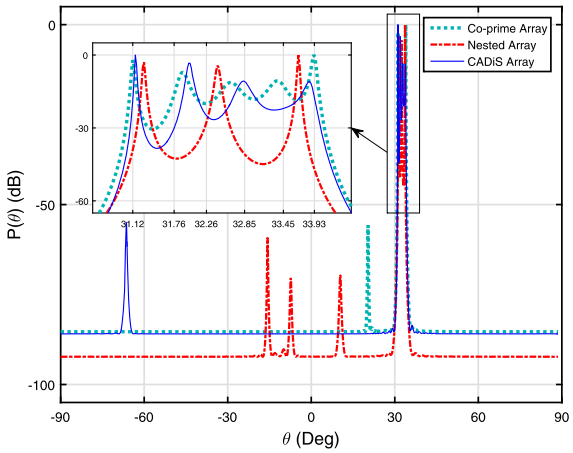

Fig. 8. The MUSIC spectra of the prior proposed coprime/nested/CADiS arrays from the environment consisting of six close sources.

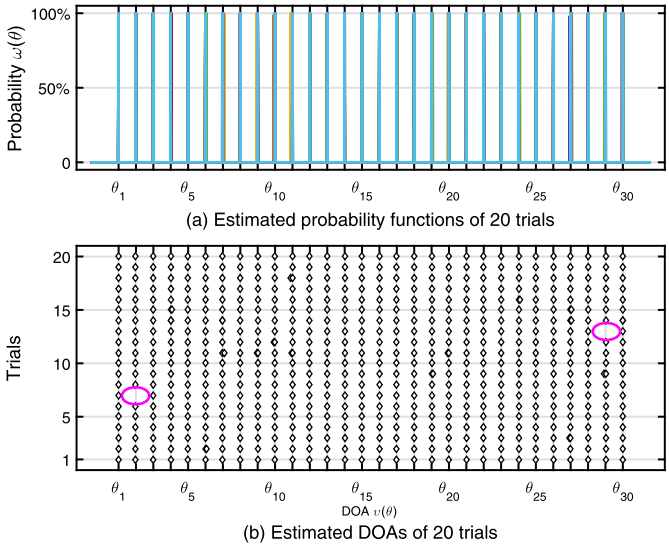

Fig. 9. The estimated results of 20 independent trails by using a 21-element K-level DisCoprime array from environment containing 30 sources: (a) the final probability function $w(\theta)$ (b) the estimated DOAs (represented by diamond $\diamond$).

As mentioned, the two kinds of K-level arrays consist of 19 and 21 sensors, respectively. For comparison, the performances of the prior Co-prime Array, Nested Array, Nested-CADiS Array consisting of 21 physical sensors from the same environment are provided in Fig. 8. It shows that the prior proposed arrays are not able to detect such six close sources, and even result in some false targets. As a conclusion, the rationality and effectiveness (especially for improving resolution) of the proposed arrays are validated experimentally.

5.2. DOF capacity

In the second experiment, we investigate DOF capacity by considering as many as 30 sources impinging on the K-level DisCoprime array in Table 2. Assuming that $\sin(\theta_i)$ of all the DOAs are uniformly distributed from -0.9 to $+0.9$, 2000 snapshots with SNR $= 15$ dB are used to obtain the covariance matrix. Other parameters are set the same as before. 20 independent trails are performed based on MUSIC algorithm, the final probability functions $w(\theta)$ and estimated DOAs are illustrated in Fig. 9, where the genuine DOAs are represented by the vectorized grid lines.

In such a situation containing more sources than sensors, generally, all the 30 sources can be clearly and correctly detected. The

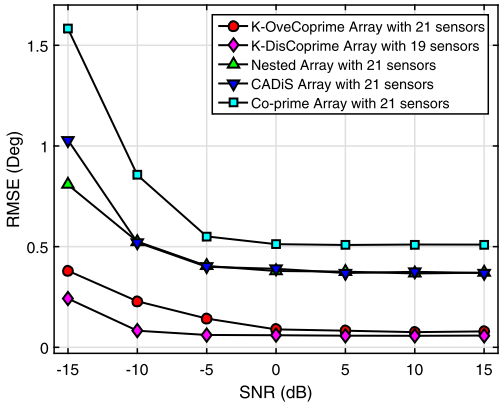

Fig. 10. The comparison of RMSEs corresponding to different SNR by using five kinds of arrays from environment consisting of eight non-uniformly distributed sources.

corresponding probability functions of 20 trails behave like a group of vertical lines, which validate the accuracy of the proposed algorithm. As a probability-based decision criterion, inevitably, the proposed algorithms may lead to the missing targets, as shown in the 7th and 13th trails. This phenomenon can be improved when a relatively loose threshold is chosen.

5.3. Estimation accuracy

The performance of DOA estimation will be further compared via Monte Carlo trials. Hence the average root-mean-square error (RMSE) of the estimated DOAs from 100 Monte Carlo trials are defined as

$$\text{RMSE} = \sqrt{\frac{1}{100D}\sum_{n=1}^{100}\sum_{k=1}^{D}\left(\hat{\theta}_k(n)-\theta_k\right)^2} \tag{28}$$

where $\hat{\theta}_k(n)$ is the estimation of θ_k for the nth trials.

In the third experiment, we compare how the SNR affects the DOA estimation accuracy. The performances of five kinds of arrays are quantified by the RMSE of 100 independent trials considering 8 sources non-uniformly distributed at $\{-60.00°, -20.00°, 20.00°, 60.00°, 31.00°, 31.50°, 32.00°, 32.50°\}$. Other parameters are set the same as before. The RMSE results corresponding to the different SNR varying from -15 dB to 15 dB are illustrated in Fig. 10. It shows that the performance of DOA estimation is improved as the increasing of the input SNR. Five kinds of arrays are able to maintain relative stable performances when SNR is higher than -5 dB. the two proposed K-level arrays can maintain good accuracy (RMSE less than $0.5°$), obviously, which outperforms the prior proposed arrays.

In the fourth experiment, we investigate the degradation of performance when the threshold ρ deviates from its optimal level. By considering the K-OveCoprime array configuration from the same signal environment in the third experiment, the performances are quantified by the probability of false/missing targets of 125 independent trials, where these two probability parameters indicate the proportion of the false/missing targets in all the 1000 targets (8×125). The results are illustrated in Fig. 11. It is observed that if ρ is set to be a higher threshold, false targets can be excluded with a higher probability, while it may result in missing some true targets. In contrast, if ρ is set to be a lower threshold, all the true targets can be detected with a higher probability, while it may result in some false targets. Anyway, generally, our proposed algorithm can maintain a relatively low false/missing target rate.

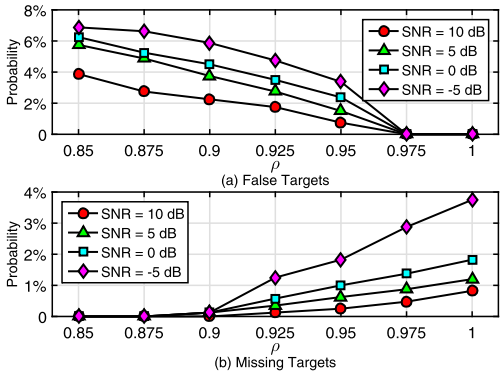

Fig. 11. The comparison of the statistical probabilities corresponding to the different SNR and different ρ: (a) the probability of false targets, (b) the probability of missing targets.

6. Conclusion

In this article, firstly, two kinds of K-level co-prime linear array geometries are proposed, where both the formation of physical array and the properties of the virtual arrays are derived with close-form expression. Compared to the prior two level co-prime/nested arrays, the aperture and the angle-resolution of the K-level array can be significantly increased with Kth power law, while the dimension of its scanning space is reduced to $1/K$ resulted from the spatial aliasing. Secondly, a class of virtual MRDCAs are generated from the vectorized covariance matrix of the measurements from the K-level arrays. A low-complexity DOA estimation algorithm is proposed by combining a multi-resolution estimation at each sparse MRDCA and a followed probability decision strategy which aims at effectively finding the genuine DOAs and excluding the replica ones. The proposed methods can not only make use of the DOFs increased by the consecutive lags, but also can fully exploit the significantly increased virtual aperture and the resolution. In the end, the simulation results are provided to numerically validate the performance of the proposed array geometries.

Appendix A. The transform function

Rectangular transform function can be expressed as

$$\mathcal{F}_{Rk}(\mathbf{P}_k, \emptyset_k) = \begin{cases} 1, & \triangle\mathbf{P}_k(\theta) \le \xi_k \\ 0, & \triangle\mathbf{P}_k(\theta) > \xi_k \end{cases} \tag{A.1}$$

where ξ_k is the cutoff threshold. The rectangular transform function possesses a flat top and can be widely used in the level with the inter-element spacing being $\frac{\lambda}{2}$.

Triangle transform function can be expressed as

$$\mathcal{F}_{\mathrm{Tk}}(\mathbf{P}_k, \emptyset_k) = \begin{cases} 1 - \frac{1-\rho}{\xi_k}\triangle\mathbf{P}_k(\theta), & \triangle\mathbf{P}_k(\theta) \le \xi_k \\ 0, & \triangle\mathbf{P}_k(\theta) > \xi_k \end{cases} \tag{A.2}$$

where ξ_k is the cutoff threshold, ρ is the cutoff threshold probability. When $\triangle\mathbf{P}_k(\theta) < \xi_k$, the triangle transform function is a linear transformation of the pseudo spectrum $\mathbf{P}_k(\theta)$.

Gaussian transform function can be expressed as

$$\mathcal{F}_{\mathrm{Gk}}(\mathbf{P}_k, \emptyset_k) = \begin{cases} e^{\frac{1}{2}(\alpha\triangle\mathbf{P}_k(\theta)/\xi_k)^2}, & \triangle\mathbf{P}_k(\theta) \le \xi_k \\ 0, & \triangle\mathbf{P}_k(\theta) > \xi_k \end{cases} \tag{A.3}$$

where ξ_k is the cutoff threshold, α is the adjusting factor, which determines the cutoff threshold probability, $\rho = e^{\frac{1}{2}\alpha^2}$.

Appendix B. Supplementary material

Supplementary material related to this article can be found online at http://dx.doi.org/10.1016/j.dsp.2016.12.002.

References

[1] R.O. Schmidt, Multiple emitter location and signal parameter estimation, IEEE Trans. Antennas Propag. 34 (3) (1986) 276–280.
[2] R. Roy, T. Kailath, ESPRIT-estimation of signal parameters via rotational invariance techniques, IEEE Trans. Acoust. Speech Signal Process. 37 (7) (1989) 984–995.
[3] A. Moffet, Minimum-redundancy linear arrays, IEEE Trans. Antennas Propag. 16 (2) (1968) 172–175.
[4] S. Pillai, Y. Bar-Ness, F. Haber, A new approach to array geometry for improved spatial spectrum estimation, Proc. IEEE 73 (10) (1985) 1522–1524.
[5] S. Pillai, F. Haber, Statistical analysis of a high resolution spatial spectrum estimator utilizing an augmented covariance matrix, IEEE Trans. Acoust. Speech Signal Process. 35 (11) (1987) 1517–1523.
[6] Y.I. Abramovich, N.K. Spencer, A.Y. Gorokhov, Detection-estimation of more uncorrelated gaussian sources than sensors in nonuniform linear antenna arrays I. Fully augmentable arrays, IEEE Trans. Signal Process. 49 (5) (2001) 959–971.
[7] P. Pal, P. Vaidyanathan, Nested arrays: a novel approach to array processing with enhanced degrees of freedom, IEEE Trans. Signal Process. 58 (8) (2010) 4167–4181.
[8] P.P. Vaidyanathan, P. Pal, Sparse sensing with co-prime samplers and arrays, IEEE Trans. Signal Process. 59 (2) (2011) 573–586.
[9] C.L. Liu, P.P. Vaidyanathan, Super nested arrays: sparse arrays with less mutual coupling than nested arrays, in: Proc. IEEE Int. Conf. Acoust., Speech, Signal Process., ICASSP, 2016, pp. 2976–2980.
[10] C.L. Liu, P.P. Vaidyanathan, Super nested arrays: linear sparse arrays with reduced mutual coupling – part I: Fundamentals, IEEE Trans. Signal Process. 64 (15) (2016) 3997–4012.
[11] S. Qin, Y. Zhang, M. Amin, Generalized coprime array configurations for direction-of-arrival estimation, IEEE Trans. Signal Process. 63 (6) (2015) 1377–1390.
[12] Q. Shen, W. Liu, W. Cui, S. Wu, Extension of co-prime arrays based on the fourth-order difference co-array concept, IEEE Signal Process. Lett. 23 (5) (2016) 615–619.
[13] C.L. Liu, P.P. Vaidyanathan, Cramér–Rao bounds for coprime and other sparse arrays, which find more sources than sensors, Digit. Signal Process. (2016), preprint.
[14] E. BouDaher, Y. Jia, F. Ahmad, M. Amin, Multi-frequency co-prime arrays for high-resolution direction-of-arrival estimation, IEEE Trans. Signal Process. 63 (14) (2015) 3797–3808.
[15] T.-J. Shan, M. Wax, T. Kailath, On spatial smoothing for direction-of-arrival estimation of coherent signals, IEEE Trans. Acoust. Speech Signal Process. 33 (4) (1985) 806–811.
[16] S.U. Pillai, B.H. Kwon, Forward/backward spatial smoothing techniques for coherent signal identification, IEEE Trans. Acoust. Speech Signal Process. 37 (1) (1989) 8–15.
[17] C.-L. Liu, P. Vaidyanathan, Remarks on the spatial smoothing step in coarray music, IEEE Signal Process. Lett. 22 (9) (2015) 1438–1442.
[18] Y.D. Zhang, M.G. Amin, B. Himed, Sparsity-based DOA estimation using co-prime arrays, in: Proc. IEEE Int. Conf. Acoust., Speech, Signal Process., ICASSP, 2013, pp. 3967–3971.
[19] N. Hu, Z. Ye, X. Xu, M. Bao, DOA estimation for sparse array via sparse signal reconstruction, IEEE Trans. Aerosp. Electron. Syst. 49 (2) (2013) 760–773.
[20] Z. Tan, Y. Eldar, A. Nehorai, Direction of arrival estimation using co-prime arrays: a super resolution viewpoint, IEEE Trans. Signal Process. 62 (21) (2014) 5565–5576.
[21] Z. Tan, A. Nehorai, Sparse direction of arrival estimation using co-prime arrays with off-grid targets, IEEE Signal Process. Lett. 21 (1) (2014) 26–29.
[22] Y. Liang, R. Ying, Z. Lu, P. Liu, Off-grid direction of arrival estimation based on joint spatial sparsity for distributed sparse linear arrays, Sensors 14 (11) (2014) 21981.
[23] D.D. Ariananda, G. Leus, Direction of arrival estimation for more correlated sources than active sensors, Signal Process. 93 (12) (2013) 3435–3448.
[24] Q. Shen, W. Liu, W. Cui, S. Wu, Y.D. Zhang, M.G. Amin, Low-complexity direction-of-arrival estimation based on wideband co-prime arrays, IEEE/ACM Trans. Audio Speech Lang. Process. 23 (9) (2015) 1445–1456.
[25] Y. Tang, Y. Lu, Multi-resolution composite array for digital beamforming with high angular-resolution, IEEE Trans. Antennas Propag. 62 (8) (2014) 4377–4380.
[26] Y. Lu, Y. Tang, H. Zhang, Thinned multi-resolution composite array for high resolution digital beamforming, in: Proc. 3rd Asia-Pacific Conf. Antennas and Propagation, APCAP, 2014, pp. 516–519.
[27] B. Liao, S.C. Chan, L. Huang, C. Guo, Iterative methods for subspace and DOA estimation in nonuniform noise, IEEE Trans. Signal Process. 64 (12) (2016) 3008–3020.
[28] C. Zhou, F. Haber, D.L. Jaggard, A resolution measure for the music algorithm and its application to plane wave arrivals contaminated by coherent interference, IEEE Trans. Signal Process. 39 (2) (1991) 454–463.
[29] J.W. Shin, Y.J. Lee, H.N. Kim, Reduced-complexity maximum likelihood direction-of-arrival estimation based on spatial aliasing, IEEE Trans. Signal Process. 62 (24) (2014) 6568–6581.

[30] Z. Weng, P.M. Djurić, A search-free DOA estimation algorithm for coprime arrays, Digit. Signal Process. 24 (2014) 27–33.

Jianyan Liu received the B.Eng. degree in information engineering from Beijing Institute of Technology, Beijing, China, in 2011. He is currently working towards the Ph.D. degree in electrical and electronic engineering. From January 2016, he was a visiting student at Nanyang Technological University (NTU) with a full financial support from China Scholarship Council. His research interests include array signal processing, direction of arrival estimation and digital beamforming based on virtual arrays.

Yanmei Zhang received the B.Eng. degree in Electromechanical Engineering from Beijing Institute of Technology in 1989, the M.Eng. degree in Mechanical and Electrical Automation from Beijing Institute of Technology in 1995 and the Ph.D. in Electromechanical Engineering from Beijing Institute of Technology in 2010, respectively. Since 1995, she has worked in School of Information and Electronics of Beijing Institute of Technology, professor, Ph.D. supervisor.

Yilong Lu received the B.Eng. degree from Harbin Institute of Technology in 1982, the M.Eng. Degree from Tsinghua University in 1984, and the Ph.D. degree from University College London (UCL) in 1991. After receiving his Ph.D. degree, he joined Nanyang Technological University (NTU), where he is currently a full Professor in the School of Electrical and Electronic Engineering. From October 1998 to June 1999, he was a Visiting Scientist at University of California - Los Angeles (UCLA).

His research interests include radar, antennas, array based signal processing, microwave techniques, computational electromagnetics, and evolutionary computation for optimization of complex problems. Dr. Lu has authored/co-authored about 300 journal and conference papers in his research areas. He is a recipient of 2012 IEEE AP-S S.A. Schelkunoff Prize Paper Award and Excellent Paper Awards from Radar 2011, Radar 2006, and IEEE MAPE 2013. Dr. Lu is a senior member of IEEE, the International Director for Singapore and a member of Nominations and Appointments Committee of IEEE Aerospace and Electronic Systems Society. He is also a member of Editorial Board for the research journal IET Radar, Sonar and Navigation.

Weijiang Wang received his B.Eng. degree and Ph.D. degree from Beijing Institute of Technology in 1999 and 2004, respectively. He is an associate professor with the School of Information and Electronics, Beijing Institute of Technology. His research interests include complex signal processing, and digital image processing.